RSC Advances

PAPER

View Article Online
View Journal | View Issue

Cite this: *RSC Adv.*, 2020, **10**, 32443

Characterization and targeting ability evaluation of cell-penetrating peptide LyP-1 modified alginate-based nanoparticles

Zhirong Zhong,[a] Liang Cai[b] and Chunhong Li *[ac]

Doxorubicin hydrochloride (DOX) shows a powerful treatment effect on breast cancer. However, for its indiscriminate distribution after systemic administration, the therapeutic response of DOX will reduce and even result in serious adverse reactions during the long-term administration. To achieve better treatment, in this study we established a non-condensing sodium alginate-based nanoparticle-encapsulated DOX (DOX/NP), the surface of which was modified with cell-penetrating peptide LyP-1 (namely LyP-1-DOX/NP) to attain active targeting towards breast cancer cells. The size of LyP-1-DOX/NP was 138.50 ± 4.65 nm, with a polydispersity index (PDI) of 0.22 ± 0.02, and the zeta potential was 18.60 ± 0.49 mV. The drug loading efficiency (DLE) for the preparation was 91.21 ± 2.01%, with an encapsulation efficiency (EE) of 12.37 ± 0.35%. The nanoparticles exhibited good stability *in vitro* and slower release trend compared with free DOX in PBS at pH7.4. *In vitro* cytopharmacodynamics showed that LyP-1-DOX/NP had an excellent anti-breast cancer effect against MDA-MB-231 cells by the MTT test. The uptake amount of LyP-1-DOX/NP by MDA-MB-231 cells was much higher than that of free DOX or unmodified DOX/NP at all time points. Further *in vivo* pharmacokinetics studies showed that the concentration of LyP-1-DOX/NP was higher than that of free DOX or DOX/NP both in plasma and in tumor, suggesting its favorable long circulation and enhancing targeting property. The present study provides a promising strategy for using the LyP-1 cell-penetrating peptide to modify nanoparticles for enhancing their targeting ability towards breast cancer.

Received 31st July 2020
Accepted 17th August 2020

DOI: 10.1039/d0ra06628a

rsc.li/rsc-advances

1. Introduction

Breast cancer is one of the most common gynecological malignancies, accounting for 7–10% of all malignant tumors.[1] It is also a serious disease, which impacts the physical and mental health of women as well as threatening their life.[2–4] Chemotherapy is an important therapeutic method for breast cancer apart from operation and radiotherapy. Doxorubicin hydrochloride (DOX), regarded as the first-line antitumor drug,[5] exhibits excellent therapeutic effects on breast cancer. However, due to its poor pharmacokinetics and non-specific distribution throughout the whole body after systemic administration as well as low penetration into tumors, DOX leads to severe toxic effects upon long-term administration.[6,7] Utilizing the targeted drug delivery system strategy is an effective way to enhance therapeutic effects and reduce the side effects by improving the penetration of drugs into tumor blood vessels and increasing its accumulation at the tumor site through the enhanced permeability and retention (EPR) effects.[8–10] The most widely DOX-encapsulated nanoparticles used in tumor treatment include liposomes, hydrogel, and metal–organic framework (MOFs). However, these nanoparticles have some defects, such as low targeting ability, a huge burst of drug release, or poor compatibility,[11–13] which prompted us to look for new nano delivery systems.

Sodium alginate, a natural polysaccharide, is a by-product of iodine and mannitol extracted from brown seaweed.[14] The molecules of sodium alginate are linked by the (1→4) bonds of β-D-mannuronic (M-block) and α-L-guluronic (G-block). For its favorable stability, solubility, biocompatible and nontoxicity, sodium alginate is widely applied in the field of medicine.[15] Furthermore, due to its low price, easy availability, biodegradability and sol–gel transition properties, alginate in the form of nanoparticles has become an ideal candidate for the delivery of numeorus drugs such as gene and chemical drugs.[16–18] To enhance drug accumulation at the tumor site and achieve active targeting ability, it is necessary to modify nanoparticles by the targeting group.

LyP-1, a cyclic peptide composed of nine amino acids (Cys–Gly–Asn–Lys–Arg–Thr–Arg–Gly–Cys), is a promising cell-penetrating homing peptide and it exhibits high specificity towards tumor

[a]*Department of Pharmaceutical Sciences, School of Pharmacy, Southwest Medical University, 3-319 Zhongshan Road, Luzhou, Sichuan, 646000, P. R. China. E-mail: lispringhong@126.com; Fax: +86 08306302050; Tel: +86 13679696586*

[b]*Nuclear Medicine Department of the First Affiliated Hospital, Southwest Medical University, Luzhou, Sichuan, 646000, P. R. China*

[c]*Engineering Research Center in Biomaterials, Sichuan University, Chengdu, Sichuan, 610064, P. R. China*

lymphatic.[19–21] It can interact selectively with tumor-associated macrophages or cancer cells in breast carcinoma by binding to its receptor p32 (gC1qR/HABP), a mitochondrial protein expressed at the surface of the cell membrane of the tumor-associated macrophage, lymphatic and cancer cells.[22,23] After binding to p32, LyP-1 could penetrate the cell membrane and enter into cytoplasm and nucleus for the targeted delivery drug to tumor sites.[22,24] As an excellent targeted group for enhancing drug accumulation at the tumor site, LyP-1 has been used in various nano preparations, such as liposomes, nanoparticles or micelles.[25,26]

In this study, we used an external gelation method to prepare and optimize DOX-loaded sodium alginate nanoparticles (DOX/NP), the surface of which was decorated with LyP-1. Utilizing electrostatic interactions between nine positively-charged NH^{2+} on the LyP-1 peptide and negatively-changed DOX/NP surface,[27] we prepared LyP-1-DOX/NP for achieving the active targeting of tumor sites. The nanoparticles can interact with cancer cells and promote phagocytosis by binding with p32 receptors on the surface of cells. Next, we studied its characteristics, *in vitro* stability, accumulative drug release, *in vitro* anticancer effect and cell uptake amount as well as *in vivo* pharmacokinetics.

2. Materials and method

2.1 Materials

LyP-1 (Cys–Gly–Asn–Lys–Arg–Thr–Arg–Gly–Cys, molecular weight 992.2, purity 98%) was bought from Zhongtai Science &Technology Co, Ltd (Shanghai, China). Medium viscosity grade sodium alginate (80–120 kDa, purity 99%), doxorubicin hydrochloride (DOX, purity ≥ 99%) and 3-(4,5-dimethylthiazol-2-yl)-2,5-diphenyltetrazolium bromide (MTT) were obtained from Solarbio Science &Technology Co, Ltd (Beijing, China). All other chemical reagents and solvents were of analytic grade or above. The chemical structures of DOX (A), sodium alginate (B) and LyP-1 (C) are shown in Fig. 1.

2.2 Cell lines and animals

MDA-MB-231 cells (Chinese Academy of Sciences, Shanghai, China) were cultured in an RPMI 1640 medium (Hyclone Laboratories, Inc., Omaha, NE) containing 10% (v/v) fetal bovine serum (GIBCO, USA) and 1% (v/v) penicillin/streptomycin (Solarbio Science & Technology Co., Ltd. Beijing, China). Cells were seeded into a culture dish, which was placed in a 5% CO_2 environment at 37 °C.

Six-week-old female Sprague-Dawley rats (200 ± 20 g) were provided by a Laboratory Animal Center of Southwest Medical University (Luzhou, China). All experimental animals were raised in common animal houses and supplied with standard feed. The indoor temperature was 25 ± 2 °C, with a relative humidity of 50 ± 10%. Animal experiments were approved by the Animal Ethics Committee of Southwest Medical University (Permit No. 20160126).

2.3 Preparation of DOX-encapsulated alginate nanoparticles

We used an external gelation method to prepare the DOX-encapsulated sodium alginate nanoparticles (DOX/NP), which were negatively charged. Briefly, 20 mL of sodium alginate (0.025% w/v) solution was pre-mixed with 1.0 mg DOX, and then 35 μL of 0.75 mM calcium chloride solution was added dropwise to the sodium alginate solution while slowing stirring it for 0.5 h, followed by Ca^{2+} ion-induced cross-linking. Next, the solution was dialyzed for 24 h and freeze-dried to gain nanoparticles. By following the same method, we prepared blank sodium alginate nanoparticles without adding DOX (SA/NP).

2.4 Preparation of LyP-1-modified DOX-encapsulated alginate nanoparticles

By charge adsorption, the surface of the above-prepared DOX/NP (0.5 mg mL^{-1}) was modified by 0.8 mg mL^{-1} of the positively charged LyP-1, with the mass ratio of LyP-1 and DOX/NP as 1 : 3. The as-prepared nanoparticles were named LyP-1-DOX/NP, and the nanoparticles were dialyzed overnight and freeze-dried (with the yield of the LyP-1-DOX/NP was 95.62%). Then, we prepared LyP-1/NP without adding DOX by the same method.

2.5 Characteristic of LyP-1-DOX/NP

Sizes, polydispersity index (PDI) and zeta potential of the LyP-1-DOX/NP were determined at 25 °C by Malvern Zetasizer Nano ZS90 (Malvern Instruments, Malvern, UK). The morphology of

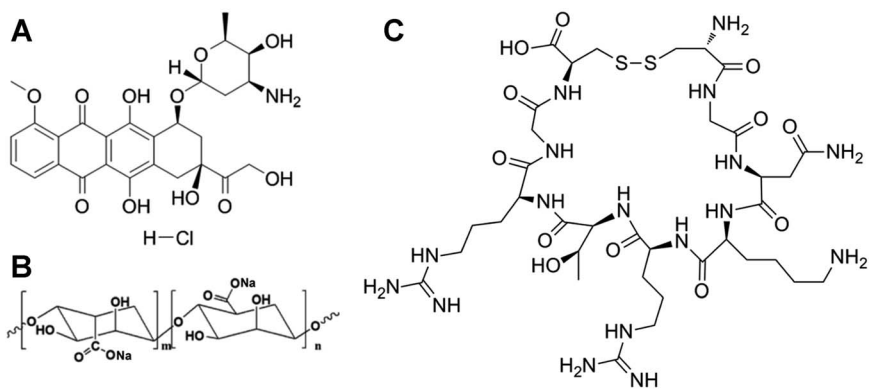

Fig. 1 The chemical structures of DOX (A), sodium alginate (B) and LyP-1 (C).

nanoparticles (1.0 mg mL^{-1}) was observed *via* transmission electron microscopy (TEM) (H-600, Hitachi, Japan) using a negative stain technique, by which samples were negatively stained and analyzed using TEM for about 30 s before the examination.

2.6 Determination of encapsulation efficiency (EE) and drug loading efficiency (DLE)

Encapsulation efficiency (EE) and drug-loading efficiency (DLE) were measured *via* the ultracentrifugation method. Briefly, 1 mL of the as-prepared nanoparticles (1.0 mg mL^{-1}) were centrifuged for 0.5 h at 10 000 rpm. Then, the supernatant was filtered using a 0.22 μm microporous membrane, and the concentration of DOX in the supernatant was determined *via* HPLC (Agilent 1260, USA). We determined the weight of the above DOX in the as-prepared total nanoparticle suspension (W_e) and the total weight of DOX (W_t) in an equal amount of the nanoparticle suspension. Finally, 1 mL of the nanoparticle suspension was dried to obtain its total weight (W_d). EE and DLE were respectively calculated using the following equations:

$$EE = W_e/W_t \times 100\%;$$

$$DLE = W_e/W_d \times 100\%.$$

2.7 *In vitro* stability of nanoparticles

In vitro stability of LyP-1-DOX/NP (1.0 mg mL^{-1}) was examined at 4 or 37 °C for 7 days. We periodically measured their size, polydispersity index (PDI) and zeta potential in the PBS solution (pH 7.4) using a Zetasizer Nano ZS90 (Malvern Instruments, UK).

2.8 Accumulative drug release of nanoparticles

We used the dialysis method to examine the *in vitro* accumulative drug release of DOX from free DOX solution, DOX/NP or LyP-1-DOX/NP. Briefly, 2 mL of free DOX solution (2.0 mg mL^{-1}) or the other two nanoparticle solutions (2.0 mg mL^{-1}) were placed into dialysis bags (MWCO 500–1000 Da). Then, the dialysis bags were dipped in PBS buffer at pH 7.4 and incubated at 37 °C with stirring at 100 rpm. At a predetermined time, 500 μL of the release medium was taken out for the HPLC analysis, and an equivalent amount of fresh buffer was added to the solution. The concentration of DOX in all samples was determined *via* HPLC within 80 h ($n = 3$).

2.9 *In vitro* antitumor assays

When the density of MDA-MB-231 cells reached 1×10^4 per well, we extracted the original medium and added 200 μL of free DOX, DOX/NP, LyP-1-DOX/NP, LyP-1/NP and SA/NP at certain concentrations (0.2, 0.4, 0.8, 1.6, 3.2, 6.4, and 12.8 μmol L^{-1}). With continuous incubation for 48 h, the number of living cells was determined using the MTT test. The relative cell viability was calculated as $([Abs]_{sample} - [Abs]_{blank})/([Abs]_{control} - [Abs]_{blank})$.

2.10 Cellular uptake assays

Free DOX (3.2 μmol L^{-1}), DOX/NP (3.2 μmol L^{-1}) or LyP-1-DOX/NP (3.2 μmol L^{-1}) was incubated with MDA-MB-231 cells for 0.5, 1, 2, or 4 h ($n = 5$). Then, the cells were washed three times with ice-cold PBS and collected for the determination of intracellular concentration by HPLC.

2.11 Pharmacokinetics study of LyP-1-DOX/NP

The pharmacokinetics study of free DOX, DOX/NP and LyP-1-DOX/NP was estimated in SD rats with the breast tumor model. To establish the tumor model, the SD rats were subcutaneously injected with 100 mg kg^{-1} of DMBA.[20] When the tumor volume reached ~1 cm^3, the rats were selected for the experiment to ensure consistency throughout the study. The selected rats were fasted and randomly divided into 15 groups ($n = 5$), and free DOX, DOX/NP or LyP-1-DOX/NP were administered to rats of random five groups in a single intravenous injection at a dose of 5 mg DOX per kg body weight. At the predetermined time (5, 10, 20, 40 and 80 min) after administrating intravenously, rats were sacrificed, and blood was collected, followed by centrifuging it at 7000 rpm for 3 min to obtain the plasma. Meanwhile, the tumor tissues were separated to homogenate to get the supernatant. Finally, the concentration of DOX in plasma samples or tumor tissues was determined *via* HPLC. Pharmacokinetic parameters of the area under the curve (AUC_{0-t}), the maximal concentration (C_{max}) and half-life period ($t_{1/2}$) of the DOX, DOX/NP and LyP-1-DOX/NP groups were estimated by DAS3.0 (Mathematical Pharmacology Professional Committee of China, Shanghai, China).

2.12 Statistical analysis

All quantitative data were expressed as mean ± SD. Statistical analysis was performed using SPSS 19.0 (IBM, Chicago, IL, USA). Differences between two groups were assessed for significance using the Student's *t*-test. Significance was determined at the following thresholds: $*p < 0.05$, $**p < 0.01$, $***p < 0.001$.

3. Results and discussion

3.1 Characteristic of DOX/NP and LyP-1-DOX/NP

The morphologies of both DOX/NP and LyP-1-DOX/NP were nearly round with an average size of about 200 nm, as shown in the TEM images (Fig. 2A and B). By performing dynamic light scattering measurements, the size of DOX/NP was found to be 167.30 ± 2.97 nm, and that of PDI was 0.25 ± 0.05 (Fig. 2C). The size of LyP-1-DOX/NP was 138.5 ± 4.65 nm, with a PDI of 0.22 ± 0.02 (Fig. 2C and D). The zeta potentials of the two preparations were −29.20 ± 0.86 mV and 18.6 ± 0.49 mV, respectively. The EE and DLE of the DOX/NP were 96.47 ± 1.03% and 14.7 ± 0.59% (Fig. 2D), respectively. In addition, the EE of LyP-1-DOX/NP was 91.21 ± 2.01%, with DLE of 12.37 ± 0.35% (Fig. 2D). By charge adsorption of the positively-charged LyP-1 and the negatively-charged DOX/NP, we prepared LyP-1-DOX/NP nanoparticles, which were more compacted than DOX/NP. It is reported that divalent cations (*e.g.*, Ca^{2+} ions) can complex with the G-blocks (α-L-guluronic) of alginate, resulting in a structure known as the

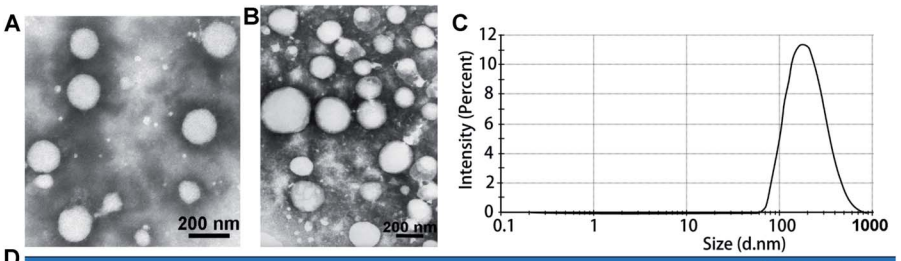

D

Parameters	Size	PDI	Zeta potential	Drug loading	Encapsulation efficiency
DOX/NP	167.30 ± 2.97	0.25 ± 0.05	-29.20 ± 0.86	96.47 ± 1.03 %	14.70 ± 0.59%
LyP-1-DOX/NP	138.50 ± 4.65	0.22 ± 0.02	18.60 ± 0.49	91.21 ± 2.01 %	12.37 ± 0.35%

Fig. 2 Morphology of DOX/NP (A) and LyP-1-DOX/NP (B) by TEM. (C) Size distribution of LyP-1-DOX/NP based on dynamic light scattering. (D) Encapsulation efficiency and drug loading efficiency of DOX/NP and LyP-1-DOX/NP ($n = 3$).

'egg-box model', in which each Ca^{2+} ion is coordinated with the carboxylate units of G-blocks. This leads to the cross-linking of alginate polymers and contributes to forming a gel-like network.[13,27] Therefore, it is interesting that the modified LyP-1-DOX/NP had a smaller size than that of DOX/NP.

Actually, we investigated the size and zeta potential of the as-prepared LyP-1-DOX/NP with different mass ratios for LyP-1 and DOX/NP, and the results verified that the nanoparticles had better distribution with 1 : 3 for LyP-1 and DOX/NP. Then, the nanoparticles were dialyzed (2000 Da MWCO) overnight and freeze-dried (the yield of the LyP-1-DOX/NP was 95.62%). Finally, we measured the concentration of the unmodified LyP-1 peptide in the discharged liquid *via* ultraviolet spectroscopy at 280 nm. The result showed that the LyP-1 in the discharged liquid was around 3% of the total peptide, suggesting that 97% of LyP-1 was used in the modification of the outer shell of the nanoparticles.

3.2 *In vitro* stability

The average size of LyP-1-DOX/NP did not obviously change over 7 days at 4 °C or 37 °C (Fig. 3A). In addition, the PDI of nanoparticles remained almost unchanged over the same period (Fig. 3B). All the results indicated that our preparation was stable in the PBS buffer, which may be due to the favorable stability of sodium alginate, facilitating its wide applications in pharmaceutical.[28] Meanwhile, this would lay the foundation for the following experiments.

3.3 *In vitro* drug release

Compared to the free drug solution, DOX was released more slowly from LyP-1-DOX/NP than DOX or DOX/NP group. By 10 h, nearly 100% of free DOX was released from the corresponding free drug solution. In contrast, only 54.30 ± 1.22% of DOX released from LyP-1-DOX/NP by 80 h (Fig. 4). These results suggested that LyP-1-DOX/NP allowed sustained drug release, which might prolong the circulation time of nanoparticles and improve its therapeutic effects. We speculated that the reason for the slower drug release of LyP-1-DOX/NP than DOX/NP might be that the DOX in the former nanoparticles needed to break through the stable charge adsorption of LyP-1 and sodium alginate. The sustained *in vitro* release of nanoparticles implied their promising potential in the circulation system.

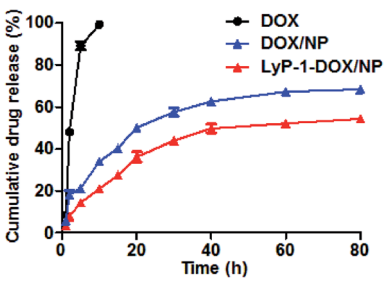

Fig. 4 *In vitro* accumulative DOX release profiles of free DOX solution, DOX/NP and LyP-1-DOX/NP at 37 °C in PBS (pH 7.4) ($n = 3$).

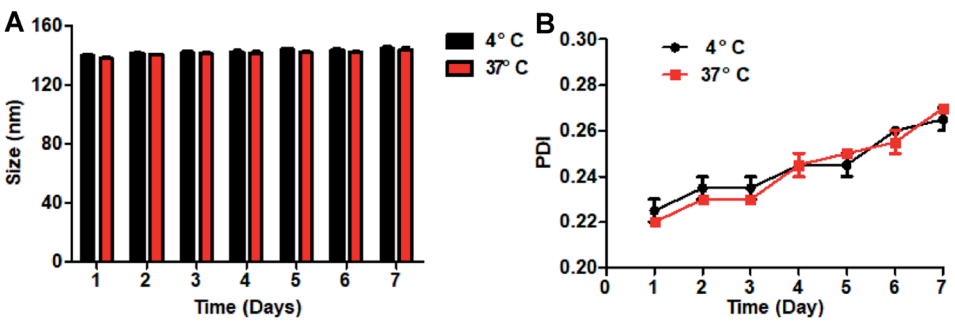

Fig. 3 (A) Size of LyP-1-DOX/NP at 4 °C or 37 °C ($n = 3$). (B) PDI of LyP-1-DOX/NP at 4 °C or 37 °C ($n = 3$).

3.4 Antitumor activity *in vitro*

Cell-penetrating peptides (CPPs) have become one of the most potent means in the area of targeted drug delivery, and the results have prompted scientists to take advantage of CPPs to achieve the treatment of tumors.[23,29] We used the MTT assay to investigate the antitumor property of LyP-1-DOX/NP.[1] It is a method of measuring cell survival and growth by the colorimetric assay, the principle of which is that succinic acid dehydrogenase can reduce exogenous MTT to form an insoluble blue-purple agent and deposit it in cells.[1] Cells were administrated with different concentrations (0.2–12.8 μmol L^{-1}) of LyP-1-DOX/NP. The results displayed that the viability of MDA-MB-231 cells reduced as the concentration of the drug increased, displaying their dose-dependent mannerism (Fig. 5A).

From the inhibition ratio *vs.* log (concentration) curve, we can see that the inhibition concentration (IC_{50} value) of LyP-1-DOX/NP against MDA-MB-231 cells was at 5.531 ± 0.47 μmol L^{-1} (Fig. 5D), which was much lower than that of DOX/NP (8.73 ± 0.96 μmol L^{-1}) and free DOX (10.51 ± 1.09 μmol L^{-1}) (Fig. 5B and C). The better *in vitro* inhibition effect of LyP-1-DOX/NP against cancer cells may contribute to preferable *in vivo* therapeutic effect.

Refer to the SA/NP and LyP-1/NP, they had no obvious effect on the viability of MDA-MB-231 cells at all concentrations, implying their nontoxicity and favorable biocompatibility.

After MDA-MB-231 cells were treated with free DOX, DOX/NP and LyP-1-DOX/NP, we determined the drug concentration of endocytosis in all groups *via* HPLC. The results exhibited that the LyP-1-DOX/NP group had the highest endocytosis at 2 h. Moreover, the uptake amount for LyP-1-DOX/NP was significantly higher than that for free DOX or DOX/NP at 2 h (Fig. 6), implying its stronger antitumor effect than other groups. This result might be ascribed to the cell-penetrating effect of the LyP-1 peptide, which could specifically recognize tumor cells and bind to the p32 receptor to enhance drug endocytosis.[25]

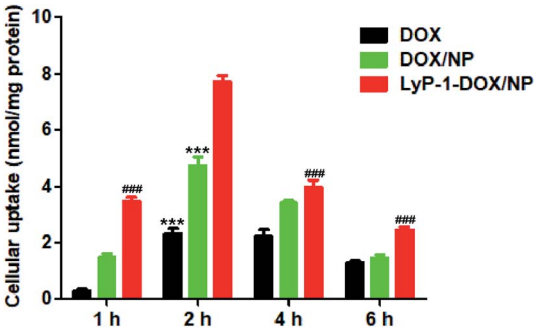

Fig. 6 The uptake amount of DOX, DOX/NP and LyP-1-DOX/NP by MDA-MB-231 cells ($n = 5$). ***$p < 0.001$ *versus* LyP-1-DOX/NP group at 2 h, $^{###}p < 0.001$ *versus* LyP-1-DOX/NP group at 2 h.

3.5 *In vivo* pharmacokinetics and targeting ability evaluation

The *in vivo* pharmacokinetic analysis results indicated that the drug concentration of LyP-1-DOX/NP in plasma was much higher than that of free DOX or DOX/NP at all-time points, suggesting improved the systemic circulation of LyP-1-DOX/NP in plasma (Fig. 7A). AUC_{0-t} of LyP-1-DOX/NP was 2.64 times of DOX and 1.26 times of DOX/NP, and its C_{max} was 2.35-fold and

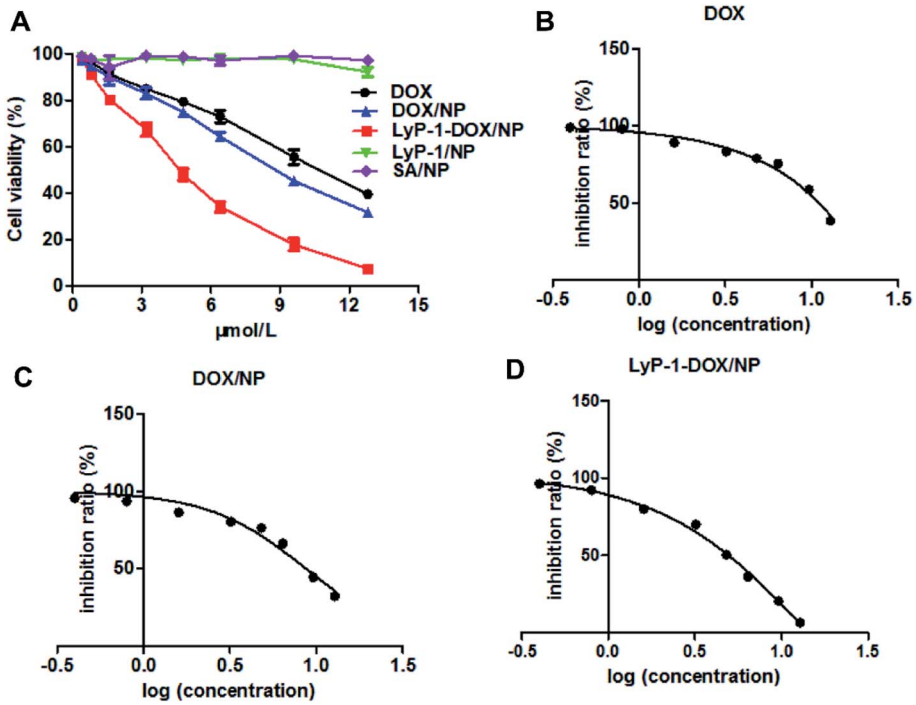

Fig. 5 *In vitro* cytotoxicity of DOX, DOX/NP, LyP-1-DOX/NP, LyP-1/NP and SA/NP against MDA-MB-231 cells. (A) MTT assays. Inhibition ratio *vs.* −log (concentration) curves of free DOX (B), DOX/NP (C) and LyP-1-DOX/NP (D).

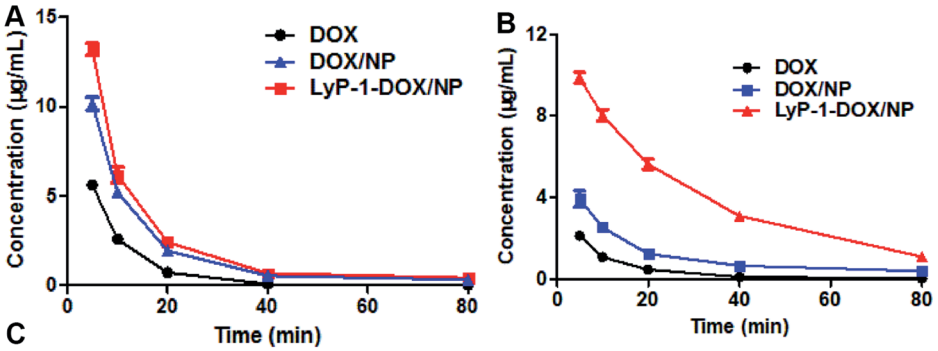

C

Pharmacokinetic parameters in plasma after i.v. injection into SD rats (n = 5).

Parameter	DOX	DOX/NP	LyP-1-DOX/NP
AUC_{0-t} (μg/mL*min)	87.22 ± 10.51	183.01 ± 9.56	229.88 ± 16.20
C_{max} (μg/mL)	5.61 ± 0.33	10.16 ± 0.80	13.21 ± 0.75
$t_{1/2}$ (min)	5.45 ± 1.26	8.60 ± 0.30	8.91 ± 0.33

Abbreviations: AUC_{0-t}: area under drug concentration-time curve, C_{max}: maximum drug concentration, $t_{1/2}$: half-life period.

Fig. 7 Concentration-*vs.*-time curves of DOX, DOX/NP and LyP-1-DOX/NP in plasma (A) or in tumor (B) and pharmacokinetic parameters in plasma (C) after intravenous injection into SD rats ($n = 5$).

1.30-fold higher than those of DOX and DOX/NP, respectively (Fig. 7C). In addition, $t_{1/2}$ of LyP-1-DOX/NP in plasma was also extended 1.63-fold and 1.04-fold than free drug and DOX/NP, respectively (Fig. 7B). All these results suggested that AUC_{0-t} and C_{max} of LyP-1-DOX/NP were both higher in plasma than those of free DOX or undecorated nanoparticles. This property may endow the nanoparticles with a long circulation feature. In addition, because of its relatively long half-life, a higher frequency of injection is not needed, which may reduce its side effect and enhance its *in vivo* antitumor effect.

To further evaluate the long circulation of DOX preparations, we investigated the amount of DOX in tumors after treatment with free DOX, DOX/NP and LyP-1-DOX/NP. The results demonstrated that the concentration of DOX in the LyP-1-DOX/NP group was much higher in tumors than that in free DOX or DOX/NP, and there were both significant differences between LyP-1-DOX/NP with other two groups, revealing the long-circulating property of LyP-1-DOX/NP (Fig. 7B).

All these results indicated that encapsulated DOX with sodium alginate could improve the bioavailability. Moreover, modifying our DOX/NP with LyP-1 led to a much greater accumulation in tumor sites than that shown by undecorated DOX/NP, and it also had higher AUC_{0-t} and C_{max} as well as longer $t_{1/2}$ in plasma than that shown by DOX/NP, which was largely due to the 'EPR' effect and the ability of LyP-1 to bind p32 specifically in disease tissues.

4. Conclusion

We successfully prepared sodium alginate nanoparticles for the delivery of DOX *via* an external gelation method. The surface of the nanoparticles was then modified by LyP-1 (namely LyP-1-DOX/NP). The LyP-1-DOX/NP showed good *in vitro* stability and sustained drug release. As shown by the MTT assay results, it exhibited an excellent anticancer effect *in vitro*. The *in vivo* pharmacokinetic research indicated that LyP-1-DOX/NP in plasma and tumor had higher AUC_{0-t}, C_{max} and $t_{1/2}$ than free DOX or DOX/NP, and these results proved the favorable targeting ability and long circulation of the prepared formulations. This study shows that modifying sodium alginate nanoparticles by LyP-1 is a promising strategy for tumor chemotherapy, offering a possible novel treatment idea for other cancers.

Conflicts of interest

The authors declare no conflict of interest.

Acknowledgements

This work is supported by the financial support of the Fund of Science and Technology Project of the Health Planning Committee of Sichuan (18ZD036), Science and Technology Project of Luzhou Government (2019-JYJ-51), Sichuan Province Science and Technology Agency Innovation Talent Project (2017RZ0048), the Transformation Project of Science and Technology Achievements of Southwest Medical University (2018002).

References

1 A. C. Gomathi, S. R. Xavier Rajarathinam, A. Mohammed Sadiq and S. Rajeshkumar, *J. Drug Delivery Sci. Technol.*, 2020, **55**, 101376.

2 Y. Okamoto, K. Taguchi, S. Imoto, V. T. Giam Chuang, K. Yamasaki and M. Otagiri, *J. Drug Delivery Sci. Technol.*, 2020, **55**, 101381.
3 F. Tian, F. Z. Dahmani, J. Qiao, J. Ni, H. Xiong, T. Liu, J. Zhou and J. Yao, *Acta Biomater.*, 2018, **75**, 398–412.
4 J. Y. Jang, J. K. Lee, Y. K. Jeon and C. W. Kim, *BMC Cancer*, 2013, **13**, 421–433.
5 D. Cao, X. Zhang, M. D. Akabar, Y. Luo, H. Wu, X. Ke and T. Ci, *Artif. Cells, Nanomed., Biotechnol.*, 2019, **47**, 181–191.
6 S. S. Timur, D. Yoyen-Ermis, G. Esendagli, S. Yonat, U. Horzum, G. Esendagli and R. N. Gursoy, *Eur. J. Pharm. Biopharm.*, 2019, **136**, 138–146.
7 T. Xue, C. Xu, Y. Wang, H. Tian and Y. Zhang, *Biomater. Sci.*, 2019, **7**, 4615–4623.
8 Y. Wan, W. Dai, R. J. Nevagi, I. Toth and P. M. Moyle, *Acta Biomater.*, 2017, **59**, 257–268.
9 D. Jiang, X. Gao, T. Kang, X. Feng, J. Yao, M. Yang, Y. Jing, Q. Zhu, J. Feng and J. Chen, *Nanoscale*, 2016, **8**, 3100–3118.
10 Q. Wang, Y. Zhong, W. Liu, Z. Wang, L. Gu, X. Li, J. Zheng, H. Du, Z. Zhong and F. Xie, *Drug Delivery*, 2019, **26**, 12–22.
11 Y. Fan, W. Wu, Y. Lei, C. Gaucher, S. Pei, J. Zhang and X. Xia, *Mar. Drugs*, 2019, **17**, 285–299.
12 S. Jain, T. H. Tran and M. Amiji, *Biomaterials*, 2015, **61**, 162–177.
13 M. Lopes, B. Abrahim, F. Veiga, R. Seica, L. M. Cabral, P. Arnaud, J. C. Andrade and A. J. Ribeiro, *Expert Opin. Drug Delivery*, 2016, **5247**, 1–14.
14 B. S. Pattni, V. V. Chupin and V. P. Torchilin, *Chem. Rev.*, 2015, **115**, 10938.
15 A. Lalloo, P. Chao and P. Hu, *J. Controlled Release*, 2006, **112**, 333–342.
16 X. Yu, A. Li, C. Zhao, K. Yang, X. Chen and W. Li, *ACS Nano*, 2017, **11**, 3990–4001.
17 S. Jain and M. Amiji, *Biomacromolecules*, 2012, **13**, 1074–1085.
18 K. I. Draget, O. Smidsrod and S. B. Gudmund, *Biopolymers Online*, 2005, vol. 1, p. 30.
19 J. D. Bjorge, A. Pang and D. J. Fujita, *PLoS One*, 2017, **12**, e0180578.
20 R. N. Gursoy and O. Cevik, *Pharm. Dev. Technol.*, 2014, 486–490.
21 S. Timur, P. Bhattarai, R. N. Gursoy, I. Vural and B. A. Khaw, *Pharm. Res.*, 2017, **34**, 352–364.
22 I. Shabo and J. Svanvik, *Adv. Exp. Med. Biol.*, 2011, **714**, 141–150.
23 C. Ciobanasu, I. Dragomir and A. Apetrei, *J. Pept. Sci.*, 2019, **25**, 3145–3155.
24 S. M. Garg, I. M. Paiva, M. R. Vakili, R. Soudy, K. Agopsowicz, A. H. Soleimani, M. Hitt, K. Kaur and A. Lavasanifar, *Biomaterials*, 2017, **144**, 17–29.
25 G. Luo, X. Yu, C. Jin, F. Yang, D. Fu, J. Long, J. Xu, C. Zhan and W. Lu, *Int. J. Pharm.*, 2010, **385**, 150–156.
26 D. Miao, M. Jiang, Z. Liu, G. Gu, Q. Hu, T. Kang, Q. Song, L. Yao, W. Li, X. Gao, M. Sun and J. Chen, *Mol. Pharm.*, 2014, **11**, 90–101.
27 S. Jain and M. Amiji, *Biomacromolecules*, 2012, **13**, 1074–1085.
28 S. Amani and Z. Mohamadnia, *Int. J. Biol. Macromol.*, 2019, **135**, 163–170.
29 O. E. Hawkins, R. S. VanGundy, A. M. Eckerd, W. Bardet, R. Buchli, J. A. Weidanz and W. H. Hildebrand, *J. Proteome Res.*, 2008, **7**, 1445–1457.